

Small-angle neutron scattering study on the stability of oxide nanoparticles in long-term thermally aged 9Cr-oxide dispersion strengthened steel

Peng-Lin Gao(高朋林), Jian Gong(龚建), Qiang Tian(田强), Gung-Ai Sun(孙光爱), Hai-Yang Yan(闫海洋),Liang Chen(陈良), Liang-Fei Bai(白亮飞), Zhi-Meng Guo(郭志猛), and Xin Ju(巨新)

Citation: Chin. Phys. B, 2022, 31 (**5**): 056102. DOI: 10.1088/1674-1056/ac43aa
Journal homepage: http://cpb.iphy.ac.cn; http://iopscience.iop.org/cpb

What follows is a list of articles you may be interested in

Surface chemical disorder and lattice strain of GaN implanted by 3-MeV Fe^{10+} ions

Jun-Yuan Yang(杨浚源), Zong-Kai Feng(冯棕楷), Ling Jiang(蒋领), Jie Song(宋杰), Xiao-Xun He(何晓珣), Li-Ming Chen(陈黎明), Qing Liao(廖庆), Jiao Wang(王姣), and Bing-Sheng Li(李炳生)

Chin. Phys. B, 2022, 31 (**4**): 046103. DOI: 10.1088/1674-1056/ac373f

In-situ TEM observation of the evolution of helium bubbles in Mo during He^+ irradiation and post-irradiation annealing

Yi-Peng Li(李奕鹏), Guang Ran(冉广), Xin-Yi Liu(刘歆翌), Xi Qiu(邱玺), Qing Han(韩晴), Wen-Jie Li(李文杰), and Yi-Jia Guo(郭熠佳)

Chin. Phys. B, 2021, 30 (**8**): 086109. DOI: 10.1088/1674-1056/abff48

Formation of nano-twinned 3C-SiC grains in Fe-implanted 6H-SiC after 1500-℃ annealing

Zheng Han(韩铮), Xu Wang(王旭), Jiao Wang(王娇), Qing Liao(廖庆), and Bingsheng Li(李炳生)

Chin. Phys. B, 2021, 30 (**8**): 086107. DOI: 10.1088/1674-1056/abff43

A revised jump-diffusion and rotation-diffusion model

Hua Li(李华), Yu-Hang Chen(陈昱沆), Bin-Ze Tang(唐宾泽)

Chin. Phys. B, 2019, 28 (**5**): 056105. DOI: 10.1088/1674-1056/28/5/056105

Recent progress on magnetic-field studies on quantum-spin-liquid candidates

Zhen Ma(马祯), Kejing Ran(冉柯静), Jinghui Wang(王靖珲), Song Bao(鲍嵩), Zhengwei Cai(蔡正蔚), Shichao Li(李世超), Jinsheng Wen(温锦生)

Chin. Phys. B, 2018, 27 (**10**): 106101. DOI: 10.1088/1674-1056/27/10/106101

Small-angle neutron scattering study on the stability of oxide nanoparticles in long-term thermally aged 9Cr-oxide dispersion strengthened steel

Peng-Lin Gao(高朋林)[1,2], Jian Gong(龚建)[2], Qiang Tian(田强)[2], Gung-Ai Sun(孙光爱)[2], Hai-Yang Yan(闫海洋)[2], Liang Chen(陈良)[2], Liang-Fei Bai(白亮飞)[2], Zhi-Meng Guo(郭志猛)[3], and Xin Ju(巨新)[1,†]

[1] *Department of Physics, University of Science and Technology Beijing, Beijing* 100083, *China*
[2] *Key Laboratory of Neutron Physics and Institute of Nuclear Physics and Chemistry, China Academy of Engineering Physics, Mianyang* 621900, *China*
[3] *Institute of Power Metallurgy, University of Science and Technology Beijing, Beijing* 100083, *China*

(Received 7 July 2021; revised manuscript received 13 December 2021; accepted manuscript online 16 December 2021)

A 9Cr-oxide dispersion strengthened (ODS) steel was thermally aged at 873 K for up to 5000 h. The size distribution and chemical composition of the dispersed oxide nanoparticles were analyzed by small-angle neutron scattering under a magnetic field. Combined with transmission electron microscopy, Vickers micro-hardness tests and electron backscattered diffraction measurements, all the results showed that the thermal treatment had little or no effect on the size distributions and volume fractions of the oxide nanoparticles in the ferromagnetic matrix, which suggested excellent thermal stability of the 9Cr-ODS steel.

Keywords: oxide dispersion strengthened (ODS) steel, small angle neutron scattering (SANS), thermal aging, nanoparticle

PACS: 61.05.fg, 68.37.Lp, 68.60.Dv **DOI:** 10.1088/1674-1056/ac43aa

1. Introduction

Oxide dispersion strengthened (ODS) steels are considered to be one of the most promising candidate structural materials for generation IV fission and fusion reactors.[1–7] Their attractiveness as nuclear structural materials lies in their excellent irradiation tolerance and creep strength at high temperature.[3–6] In comparison with conventional steels, ODS steels contain a high density of oxide nanoparticles.[7,8] These oxide nanoparticles block dislocation motion and grain boundary migration, and thus effectively increase the ultimate tensile strength and almost double the yield strength compared with conventional steels above 773 K. Therefore, the thermal stability of oxide nanoparticles in ODS steels is an important factor that directs their application.

Oksiuta *et al.*[9] and Zhong *et al.*[10] observed that the Y–Ti–O-enriched nanoparticles in 14Cr-ODS steel exhibited high stability at several annealing temperatures below 1573 K for 1 h and decreased micro-hardness above 1573 K for 1 h due to significant coarsening of the nanoparticles. Ribis *et al.*[11] suggested that the high stability of nanoparticles might be the result of a low interfacial energy. It was reported[12–14] that the Cr-rich α' phase forms in 20Cr-ODS steel and the micro-hardness is significantly increased during thermal aging at 758 K for 1000 h. Although many studies have reported on the effects of thermal aging on dispersed nanoparticles in high-Cr ODS steels, the stability of nanoparticles in 9Cr-ODS steel during long-term thermal aging has not been extensively studied.

The small-angle neutron scattering (SANS) technique is a powerful tool for probing nano-sized precipitation in ferromagnetic steels.[15–18] Because neutrons carry no charge they can penetrate deeply into bulk materials and detect buried structures. Further, neutrons have a small magnetic moment and are sensitive to magnetic structures. ODS steels can be considered as non-magnetic nanoparticles dispersed in a ferromagnetic matrix. SANS is the most convenient tool for studying this dispersion. When a saturating magnetic field is applied to the sample, statistically quantitative information about the size, shape, volume fraction and number density of the precipitate can be obtained.[19] Furthermore, additional information on the composition of the precipitates can be obtained from the ratio of magnetic scattering to nuclear scattering intensities.[14]

As reported in several papers,[20–22] the typical operating temperatures for ODS steels range from 823 K to 973 K. Throughout this work, the thermal aging temperature was set at 873 K. The stability of oxide nanoparticles in 9Cr-ODS steel during long-term thermal aging treatments up to 5000 h was studied by SANS, transmission electron microscopy (TEM) and Vickers micro-hardness measurements.

2. Experimental procedure

The 9Cr-ODS steel was prepared by mechanical alloying of a mixture of the corresponding metallic powders with

†Corresponding author. E-mail: jux@ustb.edu.cn

© 2022 Chinese Physical Society and IOP Publishing Ltd

Y_2O_3. Then the resulting mixture was consolidated by hot isostatic pressing (HIP) at 130 MPa for 4 h at 1443 K. The steel was normalized at 1323 K for 1 h followed by air-cooling, and was subsequently tempered at 1053 K for 1 h followed by air-cooling. The chemical composition of the steel used in this study is given in Table 1. Isothermal aging at 873 K was performed on the 9Cr-ODS steel for durations of 100 h, 500 h, 1000 h, 3000 h, and 5000 h under ambient pressure.

Table 1. Chemical composition of 9Cr-ODS steel (wt.%).

Fe	Cr	W	C	Ti	Ni	Si	Y_2O_3
Balance	8.88	2.10	0.13	0.16	0.067	0.072	0.35

SANS measurements of the samples were carried out at the China Mianyang Research Reactor on the Suanni small-angle neutron spectrometer. The measurements were performed using neutron wavelength (λ) of 0.53 nm and the distances between the sample and the detector were 1.9 m and 5.9 m, respectively. A scattering vector (q) range of 0.08 nm^{-1} to 2 nm^{-1} was covered. During measurements, saturated magnetic fields ($H = 1.5$ T) perpendicular to the direction of the incident neutron beam were applied to the samples. The azimuthal dependence of scattering intensities is expressed as[23]

$$I = I_{\rm nuc} + I_{\rm mag}\sin^2\alpha, \tag{1}$$

where $I_{\rm nuc}$ and $I_{\rm mag}$ are the nuclear and magnetic scattering intensity, respectively, and α is the angle between the magnetic field direction and scattering vector q. The I–q curves were radially averaged by taking 20° sectors in the horizontal ($\alpha = 0$) and vertical ($\alpha = 90$) directions of the detector plane. According to Eq. (1), the magnetic scattering intensities were calculated by $I_{\rm mag} = I(\alpha = \pi/2) - I(\alpha = 0)$. The measured data were corrected for sample transmission, background and detector efficiency. The absolute intensity was calibrated using a 1 mm thick water sample. Data reduction was processed using the program BerSANS.[24]

The TEM experiments were performed with a FEI Tecnai G20 FEG microscope at an accelerating voltage of 200 kV. Thin foils for TEM observation were mechanically polished to a thickness of about 100 μm and then electropolished by the twin-jet technique using an electrolyte consisting of 95 vol.% ethanol and 5 vol.% perchloric acid at 233 K. Electron backscattered diffraction (EBSD) analysis was performed in a field emission scanning electron microscope with a step size of 0.12 μm. The micro-hardness of these specimens was measured with a Vickers diamond pyramid under a load of 9.8 N for 10 s. Each micro-hardness value was determined through averaging 10 independent measurements of the same sample.

3. Results and discussion

3.1. Model

The ODS steel under study can be considered as a dispersion of non-magnetic spherical oxide particles in a ferromagnetic matrix. The magnetic scattering intensity from a system of polydisperse particles can be described as[25,26]

$$I(q) = (\Delta\rho_{\rm mag})^2 \int_0^\infty N(R) V_{\rm p}(R)^2 F^2(qR)\,{\rm d}R, \tag{2}$$

where $N(R)\,{\rm d}R$ is the number density of particles with a size between R and $R + {\rm d}R$ and $V_{\rm p}(R)$ is the particle volume. $F(qR)$ is the form factor of the spherical particles with radius R which can be expressed as

$$F(qR) = \frac{3\left[\sin(qR) - qR\cos(qR)\right]}{(qR)^3}, \tag{3}$$

$\Delta\rho_{\rm mag}$ is the magnetic contrast given by

$$\Delta\rho_{\rm mag} = \frac{b^{\rm p}_{\rm mag}}{v^{\rm p}_{\rm a}} - \frac{b^{\rm m}_{\rm mag}}{v^{\rm m}_{\rm a}}, \tag{4}$$

where $v^{\rm p}_{\rm a}$ ($v^{\rm m}_{\rm a}$) is the mean atomic volume of the precipitates (matrix) and $b^{\rm p}_{\rm mag}$ ($b^{\rm m}_{\rm mag}$) is the respective mean magnetic scattering length. The size distribution of the nanoparticles of the sample under study can be approximately described by a log-normal function[26]

$$N(R) = \frac{N_0}{\sigma R\sqrt{2\pi}} \exp\left[-\frac{(\ln R - \ln R_{\rm m})^2}{2\sigma^2}\right], \tag{5}$$

where $R_{\rm m}$ is the median radius, σ is the width of the size distribution and N is the number density. The mean radius of nanoparticles is evaluated as $R_{\rm m}\exp(\sigma^2/2)$. The distribution of the volume fraction of the nanoparticles is $D_{\rm v}(R) = N(R)V_{\rm p}(R)$.

The SANS magnetic scattering curves of the aged 9Cr-ODS samples are shown in Fig. 1(a). No obvious changes can be observed for q ranging from 0.3 nm^{-1} to 2 nm^{-1}, which corresponds to the scattering from the oxide nanoparticles. As q approaches 0, the form factor $F(qR)$ is close to 1, and thus $I(q)$ should become constant, which can be derived from Eqs. (2)–(5). However, as shown in Fig. 1(a), the measured magnetic scattering intensities increased at low q values, due to the scattering from large inhomogeneities at length scales larger than 30 nm (as estimated by π/q) such as carbides and magnetic domain boundaries. The low-q region ($q < 0.2$ nm^{-1}) could be fitted by a power law[27] which decays very fast toward high q. Therefore, the SANS magnetic scattering data in the measured full q range were modelled by

$$I_{\rm mag}(q) = I(q) + Bq^{-\alpha} + C, \tag{6}$$

where C is a constant that relates to the background. An example of a fitted profile is shown in Fig. 1(b). All the fitted curves matched well with the measured data.

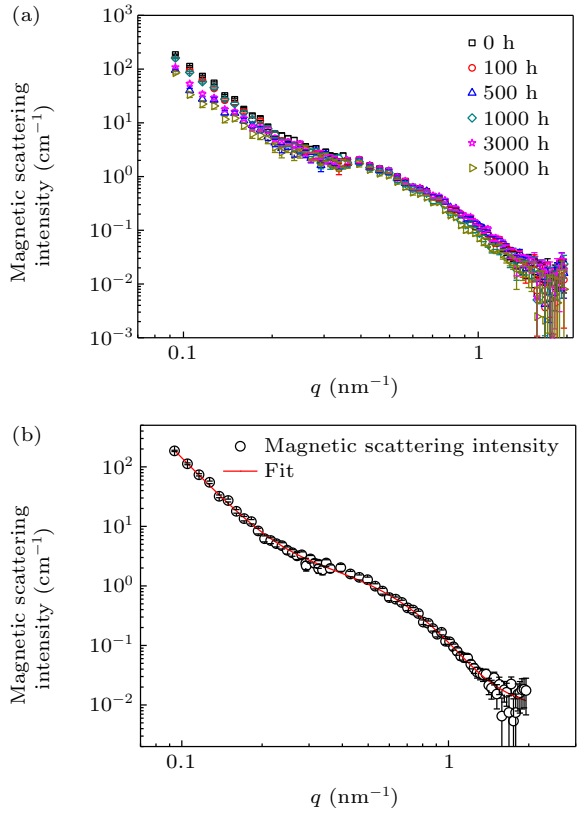


Fig. 1. (a) SANS magnetic scattering intensities for 9Cr-ODS steel for unaged sample and five different aging durations. (b) Measured (circles) and fitted (line) SANS spectra of the unaged sample.

3.2. Effects of thermal aging on oxide nanoparticles

The size distribution of oxide nanoparticles in 9Cr-ODS steel under various aging conditions is described pictorially in Fig. 2. The calculated magnetic contrast of 9Cr-ODS steel was 4.5×10^{10} cm^{-2}. The characteristics of the mean size of nanoparticles and the volume fractions are listed in Table 2. The mean radius of the precipitates of the unaged sample was 2.54 ± 0.05 nm, with a volume fraction of 0.57 ± 0.03 vol.%. For the sample aged for 5000 h, the mean radius and volume fraction of the nanoparticles were 2.52 ± 0.05 nm and 0.53 ± 0.03 vol.%, respectively. Within the uncertainties of the measurements, the fitted size distributions of all the aged samples remained unchanged.

Table 2. Characteristics of nanoparticles deduced from SANS.

Aging time (h)	Mean radius (nm)	Vol. fraction (vol.%)	A ratio
0	2.54 ± 0.05	0.57 ± 0.03	2.61 ± 0.40
100	2.49 ± 0.06	0.56 ± 0.03	2.51 ± 0.37
500	2.52 ± 0.05	0.56 ± 0.03	2.57 ± 0.42
1000	2.48 ± 0.06	0.54 ± 0.03	2.56 ± 0.41
3000	2.48 ± 0.06	0.58 ± 0.03	2.64 ± 0.40
5000	2.52 ± 0.05	0.53 ± 0.03	2.53 ± 0.40

TEM analyses were performed to cross-check the SANS results for the samples. TEM micrographs of the aged samples are shown in Fig. 3. They indicate that the oxide nanoparticles were homogenously distributed in the matrix. In this study, TEM images were analyzed using the program Nano Measurer to obtain the nanoparticle size distribution; more than 1000 particles in each specimen were statistically analyzed. Figure 4 shows the size distributions obtained by TEM and SANS techniques for the unaged and aged samples. The results are in good agreement with each other within the uncertainty of the measurements for each sample. Since the scattering intensity is proportional to the sixth power of particle size, the SANS data were weighted by the larger particles. Accordingly, the average particle size obtained from SANS is slightly larger than that derived from the TEM results.

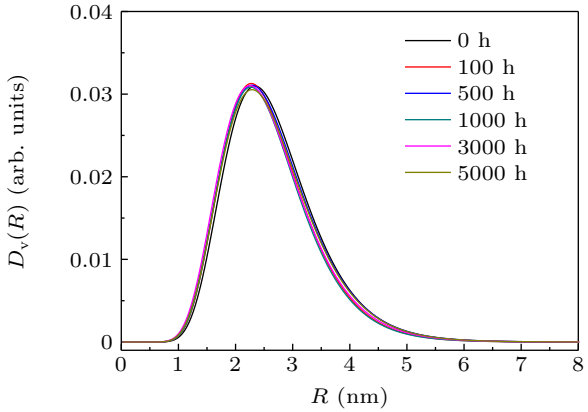


Fig. 2. Nanoparticle size distributions in thermally aged 9Cr-ODS steel.

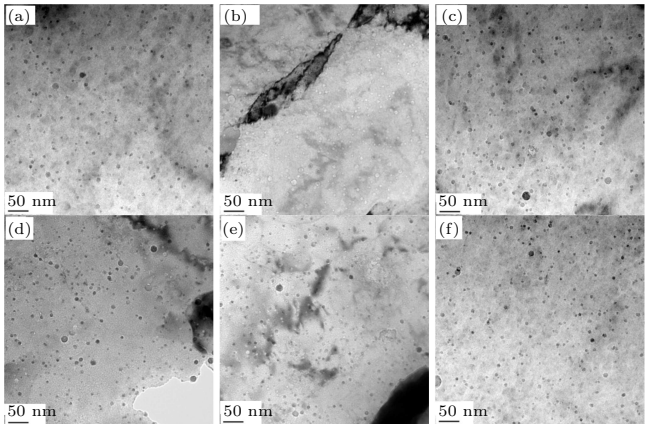


Fig. 3. TEM micrographs of 9Cr-ODS steel (a) unaged; and (b) 100 h, (c) 500 h, (d) 1000 h, (e) 3000 h, (f) 5000 h thermally aged samples.

The A ratio is defined as the ratio of normalized scattering intensities perpendicular and parallel to the magnetic field direction[28]

$$A = \frac{I_{\perp} H}{I_{//} H} = \frac{\Delta\rho^2_{\mathrm{mag}}}{\Delta\rho^2_{\mathrm{nuc}}} + 1. \tag{7}$$

This ratio was used to evaluate the chemical composition of the nanoparticles as follows. By considering only the main chemical elements, namely Fe, Cr, and W, the mean nuclear scattering lengths for the matrix were determined. The nuclear scattering lengths were calculated according to $b^{\mathrm{p,m}}_{\mathrm{nuc}} = \sum X_i b_i$, where X_i is the atomic concentration and b_i is the nuclear scattering length of the specific element.

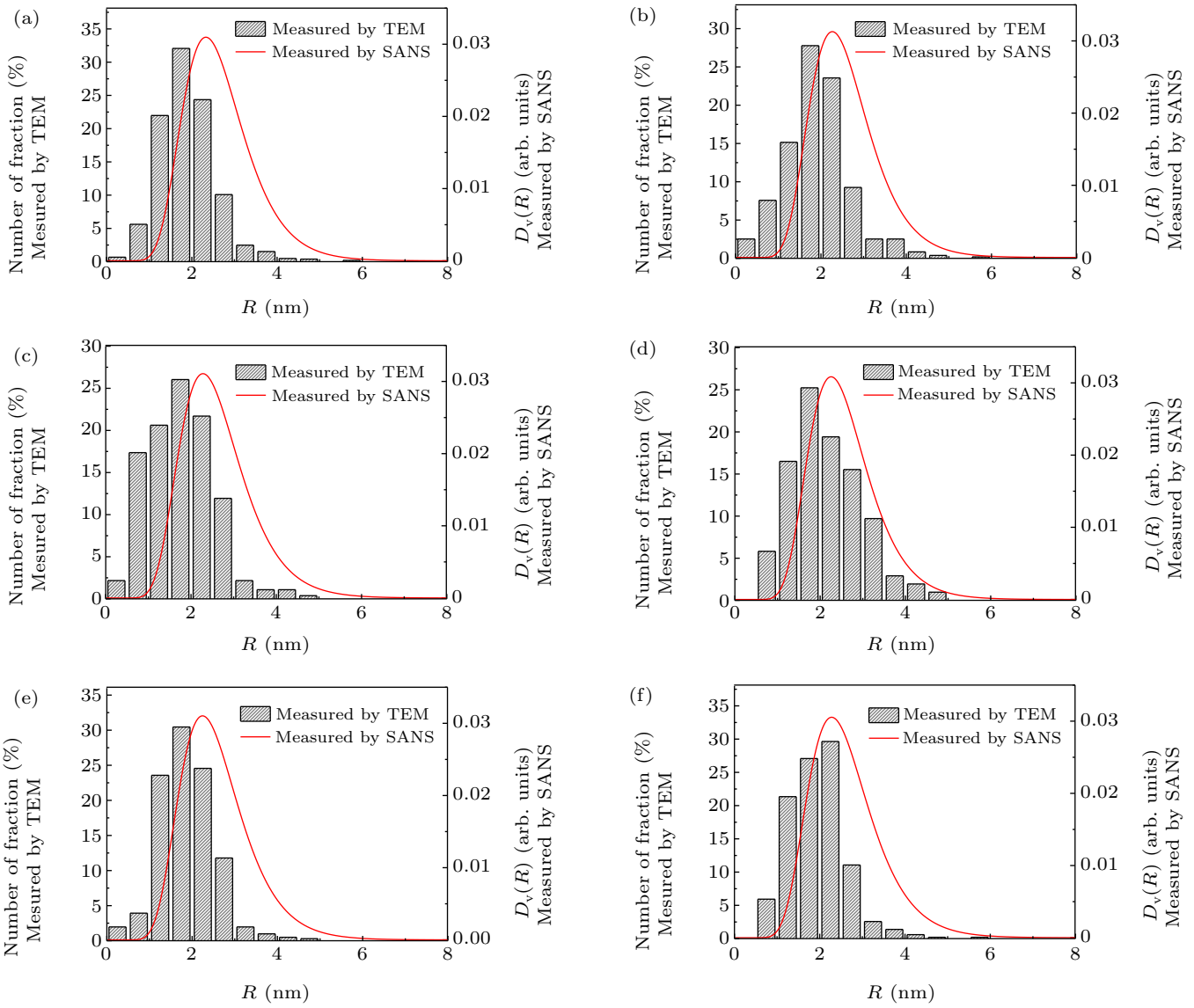


Fig. 4. Size distributions obtained by TEM and SANS for (a) unaged and (b) 100 h, (c) 500 h, (d) 1000 h, (e) 3000 h, and (f) 5000 h aged samples.

Based on the SANS study by Mathon *et al.*,[19] the nanoparticle composition for 9Cr-ODS was assumed to be $Y_2Ti_2O_7$ and the theoretical value of nuclear contrast is 3.66×10^{10} cm^{-2}. The A ratio for $Y_2Ti_2O_7$ calculated from Eq. (7) was estimated to be 2.5, in good agreement with the ratios obtained from our measurements. As shown in Table 2, the A ratio varies around 2.5 and keeps stable within the errors. Therefore, the chemical composition of the particles was not affected by the thermal treatments.

The micro-hardness of the aged samples as a function of the thermal aging time is shown in Fig. 5. The micro-hardness of the unaged sample was 365 Hv. The micro-hardness of the aged samples was found to be similar to that of the unaged samples. This relates to the high thermal stability of the extremely fine oxide nanoparticles, as evidenced by the SANS magnetic scattering and TEM results. Representative inverse pole figure (IPF) maps and the grain size distribution obtained by analyzing EBSD results of specimens aged for different times are shown in Fig. 6. The IPF maps of 9Cr-ODS steel before aging (Fig. 6(a)) and after aging up to 5000 h (Fig. 6(b)) revealed almost no change in grain structure. The average grain size before and after the aging process at 973 K for 5000 h were about 0.9 μm and 1.0 μm, respectively. The grain sizes exhibited only a slight change. This could be related to an even distribution of oxide nanoparticles, which acted to inhibit the migration of grain boundaries and dislocations during thermal aging.

In this study, the Y–Ti–O nanoparticles dispersed in 9Cr-ODS steels exhibited good stability at 873 K. In contrast to our recent work on as-milled mechanical alloyed 9Cr-ODS powders, the precipitation of nanoparticles with a radius of about 1 nm was observed by in situ SANS measurements at 873 K. In that study, prolonged annealing time or increasing temperature led to coarsening of the nanoparticles.[29] That is, the

oxide nanoparticles could precipitate in the milled ODS powder at ∼ 873 K. However, in 9Cr-ODS steel prepared by HIP at 1443 K, the nanoparticles remained stable at lower temperatures. Oono *et al.*[30] also found that the nanoparticles in 9Cr-ODS steel began to coarsen at about 1473 K during heating for 200 h, and had excellent thermal stability below 1473 K, in agreement with this work. It can be remarked here that the operating temperatures ranged from 823 K to 973 K, hence the prepared 9Cr-ODS is a potential candidate structural material for generation IV fission and fusion reactors.

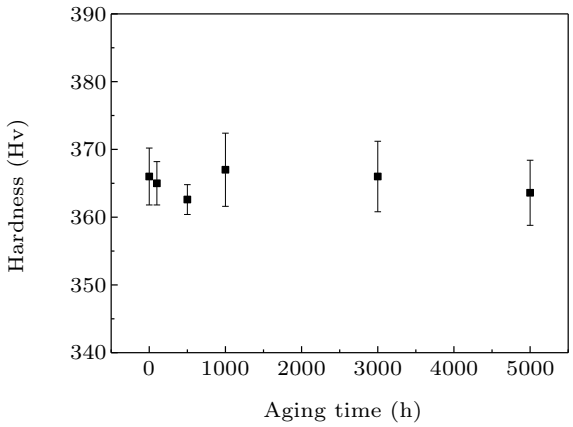


Fig. 5. Evolution of the Vickers micro-hardness measured on samples after different thermal aging treatments.

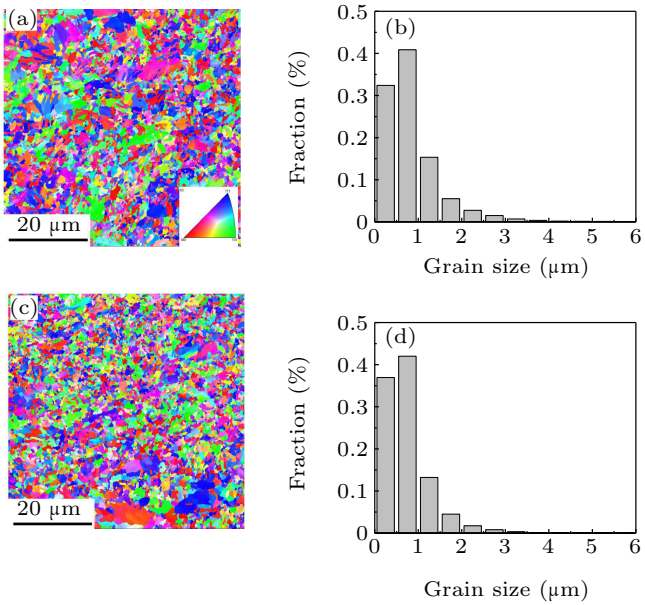


Fig. 6. Inverse pole figure maps and grain size distribution obtained by EBSD analyses for (a), (b) unaged and (c), (d) 5000 h aged samples.

The high stability of 9Cr-ODS steel is attributed to two factors. First, there is a coherent relationship between the Y–Ti–O oxide nanoparticles and the matrix, resulting in a low interfacial energy and high stability of the oxide nanoparticles.[11,31,32] Secondly, the structural stability is dependent on the Cr content in the steel. Ferritic and duplex stainless steels with a Cr content above ∼ 12 wt.% are known to harden and embrittle after thermal aging at temperatures between 673 K and 823 K due to the formation of a Cr-rich α' phase.[14,22] In this study, the 9Cr-ODS steel with a low Cr content of 8.88 wt.% showed good structural and performance stability.

In summary, the Y–Ti–O oxide nanoparticles in 9Cr-ODS steel exhibited good thermal stability after aging for 5000 h at 873 K. These nanoparticles played a key role in preventing grain growth and dislocation motion, and therefore conferred good thermal stability on the prepared 9Cr-ODS steel. The structural evolution of the Y–Ti–O nanoparticles in ODS steel at higher temperatures and longer aging times is a desirable goal for future study.

4. Conclusion

The stability of the oxide nanoparticles in 9Cr-ODS steel during thermal aging at 873 K for up to 5000 h was investigated by SANS and TEM analysis. The SANS technique showed that the size distributions of oxide nanoparticles did not change obviously after long-term thermal aging. The mean radius and volume fraction of the oxide nanoparticles in the thermally aged sample were estimated to be 2.50 nm and 0.55 vol.%, respectively. These values are in good agreement with the results obtained from TEM observations. Furthermore, no significant changes to micro-hardness and grain size were found after aging, which can be attributed to the good thermal stability of the oxide nanoparticles.

Acknowledgment

Project supported by the National Key Research and Development Program of China (Grant No. 2017YFB0702400).

References

[1] Ohtsuka S, Ukai S, Fujiwara M, Kaito T and Narita T 2004 *J. Nucl. Mater.* **329–333** 372
[2] Odette G R 2018 *Scripta Mater.* **143** 142
[3] Certain A, Kuchibhatla S, Shutthanandan V, Hoelzer D T and Allen T R 2013 *J. Nucl. Mater.* **434** 311
[4] Gao P, Ju X, Xin Y, Cao Q S, Guo Z M, Guo L P and Wang B Y 2016 *IEEE. T. Plasma. Sci.* **44** 1631
[5] Li Y F, Zhang J R, Shan Y Y, Yan W, Shi Q Q, Yang K, Shen J J, Nagasaka T, Muroga T, Yang H L, Kano S and Abe H 2019 *J. Nucl. Mater.* **517** 307
[6] Li B S, Yang Z, Xu S, Wei K F, Wang Z G, Shen T L, Zhang T M and Liao Q 2021 *Chin. Phys. B* **30** 036102
[7] Li Y F, Nagasaka T, Muroga T, Kimura A and Ukai S 2011 *Fusion Engin. Design* **86** 2495
[8] Klueh R L, Gelles D S, Jitsukawa S, Kimura A Odette G R, Schaaf B V D and Victoria M 2002 *J. Nucl. Mater.* **307–311** 455
[9] Oksiuta Z, Kozikowski P, Lewandowska M, Ohnuma M, Suresh K and Kurzydlowski K J 2013 *J. Mater. Sci.* **48** 4620
[10] Zhong S Y, Ribis J, Klosek V, Carlan Y D, Lochet N, Ji V and Mathon M H 2012 *J. Nucl. Mater.* **428** 154
[11] Ribis J, Lescoat M L, Zhong S Y, Carlan Y D and Mathon M H 2013 *J. Nucl. Mater.* **442** S101

[12] Capdevila C, Miller M K and Russell K F 2008 *J. Mater. Sci.* **43** 3889
[13] Capdevila C, Miller M K and Chao J 2012 *Acta Mater.* **60** 4673
[14] Száraz Z, Török G, Kršjak V and Hähner P 2013 *J. Nucl. Mater.* **435** 56
[15] Mathon M H, Carlan Y D, Geoffroy G, Averty X, Alaamo A and Novion C H 2003 *J. Nucl. Mater.* **312** 236
[16] Leitner H, Staron P, Clemens H, Marsoner S and Warbichler P 2005 *Mat. Sci. Eng. A* **398** 323
[17] Staron P, Jamnig B, Leitner H, Ebner R and Clemens H 2003 *J. Appl. Crystallogr.* **36** 415
[18] Zhang Z W, Yao L, Wang X L and Miller M K 2015 *Sci. Rep.* **5** 10600
[19] Mathon M H, Perrut M, Zhong S Y and Carlan Y D 2012 *J. Nucl. Mater.* **428** 147
[20] Hu H L, Zhou Z J, Li M, Zhang L F, Wang M, Li S F and Ge C C 2012 *Corros. Sci.* **65** 209
[21] Toloczko M B, Gelles D S, Garner F A Kurtz R J and Abe K 2004 *J. Nucl. Mater.* **329–333** 352
[22] Rouffié A L, Crépin J, Sennour M, Tanguy B, Pineau A, Hamon D, Wident P, Vincent S, Garat V and Fournier B 2014 *J. Nucl. Mater.* **445** 37
[23] Pareja R, Parente P, Muñoz A, Radulescu A and Castro V D 2015 *Philos. Mag.* **95** 2450
[24] Keiderling K 2002 *Appl. Phys. A* **74** s1455
[25] Jackson A J 2008 *Introduction to Small Angle Neutron Scattering and Neutron Reflectometry* p. 5
[26] Kline R S 2006 *J. Appl. Crystallogr.* **39** 895
[27] Guinier A, Fournet G, Walker C B and Vineyard G H 1956 *Phys. Today* **9** 38
[28] Coppola R, Kampmann R, Magnani M and Staron P 1998 *Acta Mater.* **46** 5447
[29] He P, Gao P L, Tian Q, Lv J M and Yao W Z 2017 *Mater. Lett.* **209** 535
[30] Oono N, Nakamura K, Ukai S, Kaito T, Torimaru T, Kimura A and Hayashi S 2016 *Nucl. Mater. Energy* **9** 342
[31] Ribis J and Carlan Y D 2012 *Acta Mater.* **60** 238
[32] Ribis J, Thual M A, Guilbert T, Carlan Y D and Legris A 2017 *J. Nucl. Mater.* **484** 183